Terahertz polarization real-time imaging based on balanced electro-optic detection

Xinke Wang,[1,2] Ye Cui,[2] Wenfeng Sun,[2] JiaSheng Ye,[2] and Yan Zhang[1,2,*]

[1]*Department of Physics, Harbin Institute of Technology, No. 92 XiDaZhiJie, Harbin 150001, China*
[2]*Beijing Key Laboratory for Terahertz Spectroscopy and Imaging, Key Laboratory of Terahertz Optoelectronics, Ministry of Education, Department of Physics, Capital Normal University, No. 105 XiSanHuan BeiLu, Beijing 100048, China*
**Corresponding author: yzhang@mail.cnu.edu.cn*

Received July 8, 2010; revised September 13, 2010; accepted September 13, 2010; posted September 21, 2010 (Doc. ID 131382); published October 11, 2010

A terahertz (THz) polarization real-time imaging system that can effectively reduce experimental time consumption for acquiring a sample's polarization information is achieved. An alternative THz polarization measurement method is proposed. In this method, a ⟨110⟩ zinc-blende crystal is used as the sensor, and the probe polarization is adjusted to detect THz electric fields on the two orthogonal polarization components. The relative sensitivity of the imaging system to the THz polarization angle is estimated to be less than 0.5°. To illustrate the ability of the system, two samples are designed and measured by using the system. From their THz polarization real-time images, each region of these samples can be precisely presented. Experimental results clearly show the special influences of different materials on the THz polarization. This work effectively extends the information content obtained by THz real-time imaging and improves the feasibility of the imaging technique.

OCIS codes: 110.6795, 300.6270, 130.5440.

1. INTRODUCTION

Terahertz (THz) real-time imaging is a powerful technique by which the THz image of a sample can be rapidly acquired and a sample's optical properties can be accurately analyzed. Many works about designs and applications of the THz real-time imaging system have been reported, such as identifying chemicals [1,2], tomography [3], and near-field imaging [4]. However, a problem of these techniques is that only one polarization component of the THz electric field is detected. The neglect may result in some difficulties to interpret THz images of materials which can influence the THz polarization. Recently, the control to the THz polarization has attracted wide research interest. Many studies about materials and devices that can change the THz polarization have been published [5–7]. Kinds of THz polarization detection methods have also been investigated, including electrical techniques [8,9] and optical techniques [10–12]. Van der Valk *et al.* first reported a THz polarization imaging method by using a ⟨111⟩ zinc-blende (ZnTe) crystal [10], and the work promoted the THz imaging into a new field. Because a ⟨110⟩ ZnTe crystal can possess higher detection sensitivity to THz signals, it has been widely used in the THz sensing and imaging. Planken *et al.* discussed the characteristics of the ⟨110⟩ ZnTe crystal in detail [13]. Zhang *et al.* achieved THz polarization images of a plastic toy by rotating the orientation of a ⟨110⟩ ZnTe crystal and calculated the Jones matrix parameters of the sample [12]. But, these imaging techniques apply the raster scanning method to build an image, so the experimental time is too long to satisfy the requirement of real applications.

A THz balanced electro-optic (EO) detection method is proposed for improving the signal-to-noise ratio (SNR) of THz real-time imaging in our latest work [14]. In this paper, a THz polarization real-time imaging system based on this technique which dramatically decreases the experimental time consumption and measures two orthogonal THz polarization components is achieved. In addition, an available THz polarization measurement approach is developed to acquire THz real-time polarization images of a sample. In this technique, a ⟨110⟩ ZnTe crystal is used as the detection sensor, and the polarization of the probe beam is adjusted to detect the polarization change of THz waves. Since the detection crystal needs not be rotated, the imaging error caused by the movement of the crystal has been effectively avoided. Compared with the method of Zhang *et al.* [12], the proposed measurement technique is more suitable to THz imaging. Two samples are designed and measured to check the ability of the proposed imaging system. In the first sample, a quartz crystal is successfully identified from other three substances, including air, a quartz glass, and a common glass by analyzing the THz polarization information. In the second sample, each region of quartz crystals with different thicknesses is accurately presented by using the same process method. The work effectively improves the feasibility of THz polarization imaging and promotes the development of the THz technology.

2. THEORY

According to [13], THz signals obtained by using the balanced EO detection technique can be expressed as

$$I(\alpha,\varphi)=I_p\frac{\omega n^3 E_{\mathrm{THz}} r_{41} L}{2c}(\cos\ \alpha\ \sin\ 2\varphi+2\ \sin\ \alpha\ \cos\ 2\varphi), \tag{1}$$

where I_p and ω are the initial power and the angular frequency of the probe beam, n is the refractive index of the detection crystal to the probe beam, r_{41} and L are the nonzero coefficient of the EO tensor and the thickness of the detection crystal, E_{THz} is the THz electric field, and c is the light speed in vacuum. The variable φ is defined as the angle between the probe polarization and the ⟨001⟩ axis of the detection crystal, and α is the angle between the THz polarization and the ⟨001⟩ axis. In the experiment, the orientation of the horizontal polarization component of the THz electric field is perpendicular to the ⟨001⟩ axis, namely, $\alpha=90°$; and that of the vertical polarization component is parallel to the ⟨001⟩ axis, namely, $\alpha=0°$. Observing Eq. (1), it can be easily concluded as

$$I(\alpha=90°,\ \varphi=0°)=2H, \tag{2}$$

$$I(\alpha=0°,\ \varphi=0°)=0, \tag{3}$$

$$I(\alpha=90°,\ \varphi=45°)=0, \tag{4}$$

$$I(\alpha=0°,\ \varphi=45°)=H, \tag{5}$$

$$H=I_p\frac{\omega n^3 E_{\mathrm{THz}} r_{41} L}{2c}. \tag{6}$$

Equations (2)–(6) show that the horizontal component of the THz electric field can be measured when the probe polarization is parallel to the ⟨001⟩ axis, and the half of the vertical component can be measured when the angle between the probe polarization and the ⟨001⟩ axis is 45°. Following the above analyses, it shows that the two polarization components of THz waves can be obtained by changing the probe polarization. It gives an effective polarization measurement method with a ⟨110⟩ ZnTe crystal. In this method, the orientation of the detection crystal needs not be changed, so the measurement accuracy is further improved.

3. EXPERIMENTAL SETUP

Figure 1 shows the optical geometry of the imaging system. The laser used is a Spectra Physics Spitfire with 1.0 kHz repetition rate, 50 fs pulse duration, 800 mW average power, and 800 nm central wavelength. Two ⟨110⟩ ZnTe crystals (10 mm × 10 mm × 3 mm) are used as the source and the detector of THz signals. We adopt a THz quasi-near-field configuration to ensure the higher imaging resolution [4]. A sample is arranged very close to the detection crystal so that the near-field information of THz waves can be detected. The probe beam passes through a polarizer and a half-wave plate (HWP) and is reflected by a 50/50 beam splitter; then it is incident on the detection crystal. In the crystal, the polarization of the probe beam is modulated by the THz electric field. The probe beam reflected by the left surface of the detection crystal passes through a quarter-wave plate, a Wollaston prism, and two lenses. After that, it is converted into two mutually orthogonal linearly polarized beams. A CY-DB1300A CCD camera (1030 × 1300 pixels, Chong Qing Chuang Yu Optoelectronics Technology Company) is used to capture the two polarization intensities of the probe beam. Every 8 × 8 pixels are combined into a new pixel for the simplification of image processing. A mechanical chopper synchronized with the CCD is utilized to extract THz signals by using the dynamic subtraction technique [15]. The synchronization frequencies of the chopper and the CCD are 25 and 2 Hz, respectively. Moreover, 100 frames are averaged for improving the SNR of THz signals. The subtraction of these two probe components is the final experimental result. The data processing method has been discussed in [14] in detail. The effect of the HWP in the probe beam is to adjust the probe polarization for measuring the polarization change of THz waves.

4. EXPERIMENTAL RESULTS AND ANALYSIS

A. Validity of the Proposed Measurement Method

To verify the ability of the proposed polarization measurement method, a THz wire grating polarizer (WG) is inserted into the THz beam and is rotated to change the THz polarization as shown in Fig. 1. The inset of Fig. 1 shows the relationship between the orientation of the WG

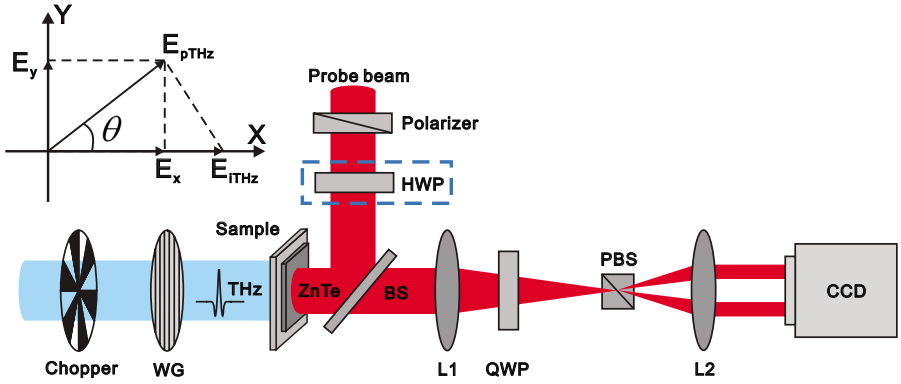

Fig. 1. (Color online) Schematic setup of the detection system: HWP, half-wave plate; BS, beam splitter; QWP, quarter-wave plate; PBS, Wollaston prism; WG, THz wire grating polarizer; L1 and L2, lenses. The inset shows the relationship between the orientation of the WG and two polarization components of THz waves.

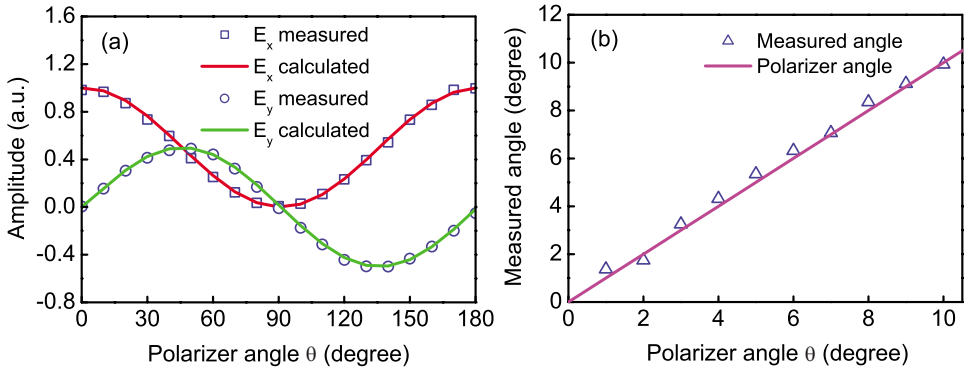

Fig. 2. (Color online) (a) Normalized transmitted THz peak amplitudes (open squares and circles) on X and Y axes as rotating the WG and theoretical results (solid red and green lines) calculated by using Eqs. (7) and (8). (b) Relative changes in the measured THz polarization angle (open triangles) for rotations of the WG by 1° steps from 0° to 10° (solid pink line).

and two THz electric field components on the horizontal (X) and vertical (Y) axes. In the experiment, it can be assumed that the initial THz polarization is horizontal, because the pump laser beam is horizontally polarized and the direction of the THz electric field generated by the optical rectification is the same as that of the pump laser beam [16]. In the inset, $E_{i\mathrm{THz}}$ is the initial THz electric field, $E_{p\mathrm{THz}}$ is the THz electric field after the WG, E_x and E_y are the projections of $E_{p\mathrm{THz}}$ on the X and Y axes, and θ is the angle of the WG with respect to the X axis. Accordingly, the expressions of E_x and E_y can be written as

$$E_x = E_{i\mathrm{THz}} \cos\theta \cos\theta, \tag{7}$$

$$E_y = E_{i\mathrm{THz}} \cos\theta \sin\theta. \tag{8}$$

The maximum amplitude of the THz signal in the time domain is measured by the imaging system, and all pixels are integrated to build a curve as θ is changing. Two polarization components of the THz signal are recorded in steps of 10° from 0° to 180°. The normalized plots and theoretical results calculated by using Eqs. (7) and (8) are shown in Fig. 2(a). The rectangular open dot and red line are the experimental and theoretical values of E_x, and the circular open dot and green line are those of E_y. Measured THz amplitudes are well coincident with the calculated results. The phenomenon exhibits two points: first, the feasibility of the measurement method is demonstrated, which can ensure that the influence of the other field component is suppressed when one field component is measured; second, the initial THz electric field possesses a well linear horizontal polarization in the experiment.

To further estimate the relative sensitivity of the imaging system to the variation of the THz polarization angle, θ is adjusted from 0° to 10° in steps of 1°, and the THz polarization angle is calculated as $\theta_{\mathrm{meas}} = \arctan(E_y/E_x)$. The measured value (trigonal open dot) and the value of θ (pink line) are shown in Fig. 2(b). The maximum deviation of the measured result θ_{meas} from the real value θ is ±0.35°. Therefore, the minimum detectable change in the polarization angle should be less than 0.5°. There are several reasons for the deviation:

(i) inhomogeneity of the THz beam spot intensity,
(ii) inhomogeneity of the probe beam spot intensity,
(iii) inhomogeneity of the electro-optical properties of the detection crystal,
(iv) imperfect quality of the WG, and
(v) precision limitation (the highest resolution is 1°) of the rotation stage which is used to mount the WG.

The polarization sensitivity can be further enhanced if the transverse distribution qualities of the THz and probe beams are improved by some methods, such as spatial filtering, and if some higher quality optical elements are used.

B. THz Temporal Signals and Spectra of Samples

To check the ability of the imaging system, we use the system to successfully identify a quartz crystal from other three types of substances (air, quartz glass, and common glass). A 0° cut quartz crystal with 3 mm thickness is chosen as the polarizing device to compare with air, a quartz glass with 1 mm thickness, and a common glass with 2 mm thickness. In the experiment, the azimuth angle of the quartz crystal is carefully optimized for ensuring the larger component on the vertical direction. The angle between the crystalline axis of the quartz crystal and the X axis is about 40°. First of all, the four materials are measured by using a standard THz time domain spectroscopy system, and the proposed method is used to detect two THz polarization components as shown in Fig. 3. In these plots, the blue dashed lines and red solid lines represent the horizontal and vertical THz polarization components, respectively. The vertical components are multiplied by 2 to match the horizontal components by virtue of Eq. (5). Figure 3(a) shows the THz temporal signals in the air in which the difference between the peak amplitudes of the two polarization components is very obvious. Their ratio is 50:1, which also indicates that the polarization of the incident THz waves is well horizontally linear and agrees with the measurement results in Fig. 2. Figures 3(b) and 3(c) are the transmitted THz signals from a quartz glass and a common glass. Although the differences of amplitudes and time shifts of these signals are very obvious due to these materials' different absorptions, refractive indices, and thicknesses, the ratios of their two polarization components hardly change. Because these two

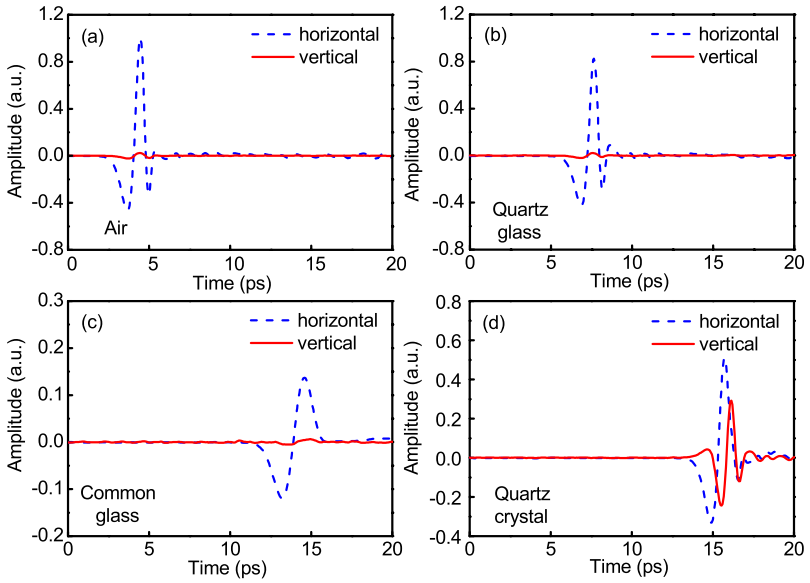

Fig. 3. (Color online) (a) THz temporal signal in the air, and (b)–(d) transmitted THz signals after passing through a quartz glass, a common glass, and a quartz crystal. The blue dashed lines and the red solid lines are the horizontal and the vertical THz electric fields, respectively.

glasses have no specific crystalline orientation, they are the isotropic materials to THz waves and do not influence the THz polarization. Figure 3(d) shows the transmitted THz signals from the quartz crystal. It can be clearly observed that the vertical component is significantly higher than that of other materials. Observing these two signals, it can be found that their peak positions are not overlapping each other, which are 15.7 ps for the horizontal component and 16.2 ps for the vertical component. According to [17], the refractive index of the extraordinary wave in the quartz crystal is from 2.153 to 2.163 in the 0.2–2.0 THz range; that of the ordinary wave is from 2.106 to 2.114. Moreover, the refractive index difference between the two polarization components almost remains constant with the frequency. Utilizing the formula $\Delta n \times d/c$, where Δn is the refractive index difference and d is the thickness of the sample, the time delay between two polarization components can be evaluated as 0.49 ps, which is approximately equal to the experimental result.

These THz temporal signals are performed by the Fourier transform, and their energy ratios in the two components are calculated in the 0.05–2.10 THz range as illustrated in Fig. 4. In this figure, the differences between the spectral intensities of two components are plotted, normalized to the sum of these two intensities. The ratios of the air and the quartz glass are almost a constant at 1, which shows that these two substances do not change the THz polarization. The ratio of the common glass also keeps a steady value of 1 below 0.80 THz, but its data are not available above 0.80 THz due to the strong absorption. In the plot of the quartz crystal, it can be seen that the ratio gradually decreases from 0.05 to 1.15 THz, then increases from 1.15 to 2.10 THz again. At 1.15 THz, there is a maximum of the THz vertical component. According to the birefringence model, the expressions of the horizontal and the vertical components of THz waves propagating through a birefringence device can be written as

$$E'_x = E_{i\mathrm{THz}}\left[\cos\left(\frac{\omega\Delta n d}{2c}\right) + j\,\sin\left(\frac{\omega\Delta n d}{2c}\right)\cos(2\beta)\right], \quad (9)$$

$$E'_y = E_{i\mathrm{THz}}\left[j\,\sin\left(\frac{\omega\Delta n d}{2c}\right)\sin(2\beta)\right], \quad (10)$$

where β is the angle between the crystalline axis of the birefringence sample and the X axis. Utilizing Eqs. (9) and (10), the energy ratio is calculated and is shown in Fig. 4. The tendency and the peak position of the curve well agree with that of the quartz crystal. Their difference is due to the reason that the absorption of the quartz crystal to THz waves and other experimental errors are not considered in Eqs. (9) and (10). According to the above analyses, the difference of the quartz crystal's optical properties compared with other samples can be well recognized by analyzing their polarization information.

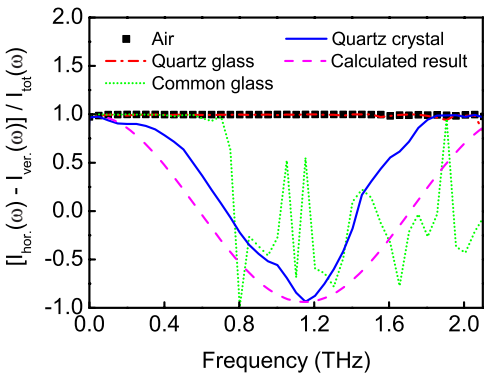

Fig. 4. (Color online) Relative intensity differences between the two THz polarization components as a function of frequency for propagation through the air, the quartz glass, the common glass, and the quartz crystal. The purple dashed line is the calculated result by using Eqs. (9) and (10).

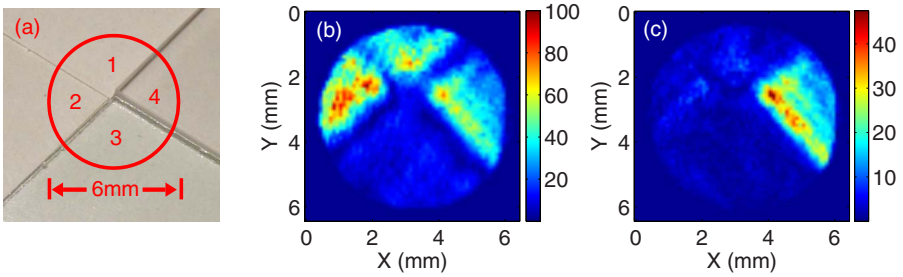

Fig. 5. (Color online) (a) Photo of the samples, including 1. air, 2. quartz glass, 3. common glass, and 4. quartz crystal. (b) and (c) are transmitted THz intensities on the horizontal and vertical polarization vectors at 0.55 THz.

C. THz Real-Time Images of Samples

The advantage of THz polarization real-time imaging is that it can quickly acquire polarization information of a sample on a large imaging area. Because the used CCD is not a fast one, the total experimental time is about 4 h. However, the time consumption can be expected to be reduced to several minutes if a fast CCD is used. In the conventional raster scanning method, it may spend about several days on the same experiment, so the real-time imaging technique is a more practical method in real applications. Four samples are arranged in the system, and their photos are presented in Fig. 5(a). The area in the red circle with 6 mm diameter is the imaging region. It is not easy to identify the quartz crystal from other two glasses because all of them are colorless and transparent. Our imaging system is used to obtain the THz images of these samples on two polarization components. Spectral information of THz images is obtained by performing the Fourier transformation of the temporal signal on each pixel. For ensuring the enough SNR in each region of the sample, spectral images of the horizontal and vertical components at 0.55 THz are extracted as shown in Figs. 5(b) and 5(c). In Fig. 5(b), the transmissivities of the air, the quartz glass, and the quartz crystal are almost the same and that of the common glass is obviously lower than other materials' due to its higher absorption. Clearly, the quartz crystal cannot be recognized in this figure. In Fig. 5(c), it can be easily seen that the intensities in the air, the quartz glass, and the common glass parts are very weak and that of the quartz crystal part is evidently higher than others' because its birefringence property increases the proportion of the THz vertical polarization component. To further characterize the property of the quartz crystal, the energy ratio and polarization angle θ_{meas} at 0.55 THz are calculated by utilizing Figs. 5(b) and 5(c) as shown in Figs. 6(a) and 6(b). The background of the image is set to zero for clarity. In Fig. 6(a), the ratios in the regions of the air, the quartz glass, and the common glass are almost 1 and that of the quartz crystal part is approximately 0.48, which are in well accordance with the results in Fig. 4. In Fig. 6(b), the polarization angle in the quartz crystal part is about 33° and that of others is about 2°. In addition, some slight noises in these two figures are attributed to the diffraction of THz waves at the edges of these samples. The quartz crystal can be clearly recognized from Figs. 6(a) and 6(b). These results indicate that the change in the THz intensity is mainly due to the sample's birefringence and is not due to the absorption.

To further describe the power of the proposed imaging system, the second sample is designed by using two pieces of quartz crystal with 1.5 mm thickness. A quartz crystal is laid partly overlapping the other, and the imaging region is the area in the red circle with 6 mm diameter as shown in Fig. 7(a). The directions of their crystalline axes are parallel. The angle between the direction and the X axis is about 45°. To enhance the contrast of THz images, spectral intensities integrated between 0.65 and 0.85 THz on two polarization components are extracted, and the energy ratio and the polarization angle are calculated by using the same process method of Fig. 6. The experimental results are shown in Figs. 7(b) and 7(c). From these two figures, it can be seen that the ratio and the angle in the two pieces of quartz crystal region are about 0.3 and 38°, and those of one piece of quartz crystal are about 0.8 and 20°. These results clearly show that quartz crystals with different thicknesses induce different influences to THz polarization. The thicker quartz crystal causes more proportion of the THz vertical component. Each region of the second sample can be accurately identified from Figs. 7(a) and 7(b). According to the above analyses, the power of the imaging system has been well demonstrated. Our results indicate that optical features of a material need to be analyzed on two polarization vectors at same times. Some important optical information may be neglected with a measurement of only one electric field component.

Recently, the polarization modulations of surface plasmon polaritons [18] and metamaterials [11,19] on THz waves have inspired great interest in the fundamental research field. On the other hand, it has been demonstrated that the THz near-field imaging techniques can become a powerful tool to present the modulation properties of these samples on the two-dimensional range [18,20,21]. Our recent works have achieved the real-time and balanced detection of the THz near-field imaging technique

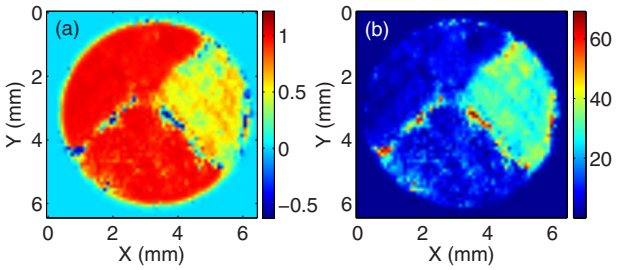

Fig. 6. (Color online) Distributions of (a) the energy ratio and (b) the polarization angle at 0.55 THz obtained by processing Figs. 5(b) and 5(c).

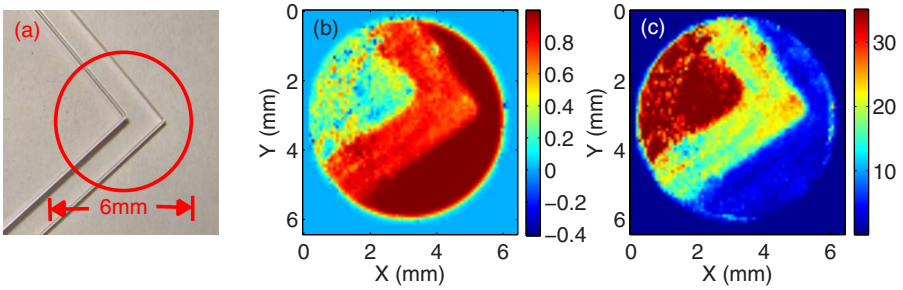

Fig. 7. (Color online) (a) Photo of the second sample. (b) and (c) are distributions of the energy ratio and the polarization angle of the second sample in the two polarization components.

[3,4]. In this paper, this imaging technique is improved to achieve the THz polarization detection with high resolution and high SNR. Because the THz polarization is measured by changing the probe polarization instead of rotating the detection crystal, the alignment of the optical system is not influenced so that the measurement accuracy is greatly advanced. We absolutely believe that the work can provide a valuable method for studying the special modulation effect of surface plasmon polaritons and metamaterials on electromagnetic waves in the microscopic scale. In addition, the birefringence of some plant fibers to THz waves has also been reported [6]. Our work can provide a "THz real-time microscope" for studying the internal structures of these plants.

5. CONCLUSION

In conclusion, a THz polarization real-time imaging system is achieved, which significantly improves the availability of THz polarization imaging. A THz polarization measurement method is proposed, and its principle is discussed in detail on the theory and experiment. Successfully characterizing the different modulations of two samples to THz polarization, the feasibility of the imaging system is well demonstrated. The introduction of THz polarization information into real-time imaging effectively improves the practicability of THz real-time imaging techniques. The work promotes the development of THz imaging in biological imaging and fundamental research fields.

ACKNOWLEDGMENTS

This work was supported by the National Basic Research Program of China (grants 2006CB302901 and 2007CB310408), the National Natural Science Foundation of China (NSFC) (grants 10604042 and 10674038), the Funding Project for Academic Human Resources Development in Institutions of Higher Learning under the Jurisdiction of Beijing Municipality, and the Science and Technology Program of Beijing Educational Committee (grant KM200810028008).

REFERENCES

1. M. Usami, M. Yamashita, K. Fukushima, C. Otani, and K. Kawase, "Terahertz wideband spectroscopic imaging based on two-dimensional electro-optic sampling technique," Appl. Phys. Lett. **86**, 141109 (2005).
2. H. Zhong, A. Redo-Sanchez, and X.-C. Zhang, "Identification and classification of chemicals using terahertz reflective spectroscopic focal-plane imaging system," Opt. Express **14**, 9130–9141 (2006).
3. X. K. Wang, Y. Cui, W. F. Sun, Y. Zhang, and C. L. Zhang, "Terahertz pulse reflective focal-plane tomography," Opt. Express **15**, 14369–14375 (2007).
4. X. K. Wang, Y. Cui, D. Hu, W. F. Sun, J. S. Ye, and Y. Zhang, "Terahertz quasi-near-field real-time imaging," Opt. Commun. **282**, 4683–4687 (2009).
5. J.-B. Masson and G. Gallot, "Terahertz achromatic quarter-wave plate," Opt. Lett. **31**, 265–267 (2006).
6. M. Reid and R. Fedosejevs, "Terahertz birefringence and attenuation properties of wood and paper," Appl. Opt. **45**, 2766–2772 (2006).
7. C.-F. Hsieh, Y.-C. Lai, R.-P. Pan, and C.-L. Pan, "Polarizing terahertz waves with nematic liquid crystals," Opt. Lett. **33**, 1174–1176 (2008).
8. H. Makabe, Y. Hirota, M. Tani, and M. Hangyo, "Polarization state measurement of terahertz electromagnetic radiation by three-contact photoconductive antenna," Opt. Express **15**, 11650–11657 (2007).
9. E. Castro-Camus, J. Lloyd-Hughes, L. Fu, H. H. Tan, C. Jagadish, and M. B. Johnston, "An ion-implanted InP receiver for polarization resolved terahertz spectroscopy," Opt. Express **15**, 7047–7057 (2007).
10. N. C. J. van der Valk, W. A. M. van der Marel, and P. C. M. Planken, "Terahertz polarization imaging," Opt. Lett. **30**, 2802–2804 (2005).
11. N. Kanda, K. Konishi, and M. Kuwata-Gonokami, "Terahertz wave polarization rotation with double layered metal grating of complimentary chiral patterns," Opt. Express **15**, 11117–11125 (2007).
12. R. X. Zhang, Y. Cui, W. F. Sun, and Y. Zhang, "Polarization information for terahertz imaging," Appl. Opt. **47**, 6422–6427 (2008).
13. P. C. M. Planken, H.-K. Nienhuys, H. J. Bakker, and T. Wenckebach, "Measurement and calculation of the orientation dependence of terahertz pulse detection in ZnTe," J. Opt. Soc. Am. B **18**, 313–317 (2001).
14. X. K. Wang, Y. Cui, W. F. Sun, J. S. Ye, and Y. Zhang, "Terahertz real-time imaging with balanced electro-optic detection," Opt. Commun., in press; available online.
15. Z. P. Jiang, X. G. Xu, and X.-C. Zhang, "Improvement of terahertz imaging with a dynamic subtraction technique," Appl. Opt. **39**, 2982–2987 (2000).
16. Q. Chen, M. Tani, Z. P. Jiang, and X. C. Zhang, "Electro-optic transceivers for terahertz-wave applications," J. Opt. Soc. Am. B **18**, 823–831 (2001).
17. D. Grischkowsky, S. Keiding, M. van Exter, and Ch. Fattinger, "Far-infrared time-domain spectroscopy with terahertz beams of dielectrics and semiconductors," J. Opt. Soc. Am. B **7**, 2006–2015 (1990).
18. M. A. Seo, A. J. L. Adam, J. H. Kang, J. W. Lee, S. C. Jeoung, Q. H. Park, P. C. M. Planken, and D. S. Kim, "Fourier-transform terahertz near-field imaging of one-dimensional slit arrays: mapping of electric-field-, magnetic-field-, and Poynting vectors," Opt. Express **15**, 11781–11789 (2007).
19. P. Weis, O. Paul, C. Imhof, R. Beigang, and M. Rahm,

"Strongly birefringent metamaterials as negative index terahertz wave plates," Appl. Phys. Lett. **95**, 171104 (2009).
20. A. J. L. Adam, J. M. Brok, M. A. Seo, K. J. Ahn, D. S. Kim, J. H. Kang, Q. H. Park, M. Nagel, and P. C. M. Planken, "Advanced terahertz electric near-field measurements at sub-wavelength diameter metallic apertures," Opt. Express **16**, 7407–7417 (2008).
21. M. A. Seo, A. J. L. Adam, J. H. Kang, J. W. Lee, K. J. Ahn, Q. H. Park, P. C. M. Planken, and D. S. Kim, "Near field imaging of terahertz focusing onto rectangular apertures," Opt. Express **16**, 20484–20489 (2008).